CHAPTER IV

IMPROVEMENT OF SULFONATED POLYSULFONE MEMBRANE FOR DIRECT METHANOL FUEL CELL: EFFECT OF ZEOLITE Y AND SULFONATED GRAPHENE OXIDE

4.1 Abstract

The proton exchange membranes (PEMs) are being developed intensively due to their great potential as a promising power source for transportation, residential, and portable applications. In this work, the novel PEMs consisting of inorganic fillers embedded in sulfonated polysulfone (S-PSF) were fabricated. The effect of zeolite Y and sulfonated graphene oxide (S-GO) was investigated on the thermal and mechanical stability, water uptake, proton conductivity, and methanol permeability. The proton conductivity of S-PSF/zeolite Y membrane increased with increasing zeolite Y content, in parallel with the methanol permeability. It was due to its water retention property. With S-GO addition, the highest proton conductivity was found at 3 % v/v of S-GO because of the increment of sulfonic acid groups by incorporating of S-GO. The S-GO particles positively affected the blocking of water and methanol molecules, caused by the increase in interfacial interaction between S-PSF and S-GO, leading to the decreases in the water uptake and methanol permeability. In addition, the hybrid membranes namely the S-PSF membrane mixed with both zeolite Y and S-GO, were also investigated. They showed better performances than the pristine S-PSF and Nafion117 membrane. All composite membranes are potential candidates for being used in DMFC applications.

Keywords: Direct Methanol Fuel Cell, Sulfonated Polysulfone, Zeolite Y, Sulfonated Graphene Oxide, Proton Exchange Membrane

4.2 Introduction

The direct methanol fuel cell (DMFC) is strongly considered as one of the most promising power sources for portable or mobile power due to its advantages such as high energy efficiency, ease of handling, low operating temperature, and environmental friendly (Ahmad *et al.*, 2010 and Auimviriyavat *et al.*, 2011). The proton exchange membrane (PEM) is considered to be an important part in DMFC where they should have the required properties; high proton conductivity under operating temperature, good mechanical and chemical stabilities for long term, resistance to swelling, low methanol crossover, and low cost. The most widely used PEM for DMFC is Nafion, a perfluorsulfonic acid polymer produced by Dupont. Nafion exhibits excellent proton conductivity (~0.1 S/cm) at ambient temperature (Qiao *et al.*, 2005), high mechanical and chemical stabilities (Wootthikanokkhan *et al.*, 2006). However, its high cost, high methanol crossover and low cell performance under low humidity or high temperature have limited its wide commercialization (Devrim *et al.*, 2009). These drawbacks of Nafion have motivated the development of new membrane materials for DMFCs. Several researches have been reported on sulfonated polymers used as a PEM. The sulfonation process enhances the hydrophilic pathway for proton transfer within a polymer matrix by attaching sulfonic groups ($-SO_3H$) on its polymer backbone. There were many sulfonated polymers such as poly (ether ether ketone) (Macksasitorn *et al.*, 2012), poly(phenylene) (Ghassemi *et al.*, 2004; Kobayashi *et al.*, 1998), poly(arylene ether) (Gao *et al.*, 2005; Wang *et al.*, 2001), polyimides (Chen *et al.*, 2007; Miyatake *et al.*, 2007), polysulfone (Unnikrishnan *et al.*, 2012), and polyvinylidene (Macksasitorn *et al.*, 2012).

Polysulfone (PSF) is one of the preferred materials due to its low cost, high thermal stability, and easy availability. In addition, this polymer has been easily sulfonated with various sulfonating agents giving excellent proton conducting membranes (Unnikrisnan *et al.*, 2012; Devrim *et al.*, 2009). The sulfonated polysulfone (S-PSF) is expected to have a good proton conductivity and thermal stability. To further improve the properties of S-PSF membrane, the polymer/inorganic composite membranes have attracted attention. The membranes

can be incorporated with inorganic fillers, such as titanium dioxide (Devrim *et al.*, 2009), cloisite 30B (Unnikrisnan *et al.*, 2012), silica (Lufrano *et al.*, 2006; Lufrano *et al.*, 2008; Lufrano *et al.*, 2012), and zeolite (Auimviriyavat *et al.*, 2011; Yildirim *et al.*, 2009). Zeolite Y is a good candidate as hydrophilic inorganic filler for polymer membrane and has been reported to be an ion conductor as well as it possesses excellent thermal and mechanical properties (Ahmed *et al.*, 2006). Similarly, the materials based on graphene oxide (GO) as inorganic fillers in polymer composites have also been of interest, due to their high aspect ratio, high conductivity, high mechanical strength and electrical insulating property (Heo *et al.*, 2012). This material has been used as inorganic filler in composite membrane to improve the mechanical strength, water retention in the membrane, proton conductivity, and methanol permeability.

In this work, PSF was sulfonated with concentrated sulfuric acid and confirmed by ^{1}H-NMR and FT-IR spectroscopy. The composite membranes were incorporated with zeolite Y and S-GO as inorganic fillers in S-PSF through solution casting process. The effect of filler loading was evaluated. The proton conductivity and methanol permeability of the fabricated composite membranes were favorably compared with those of pristine S-PSF and a commercial membrane Nafion117.

4.3 Experimental

4.3.1 Materials

Polysulfone (PSF; Aldrich) was used as the polymer based membrane. Concentration sulfuric acid (98%) (H_2SO_4; Univar, Ar grade) was used as a sulfonating agent. Dichloromethane (DCM; RCI Labscan, AR grade), and dimethylacetamide (DMAc; RCI Labscan, AR grade) were used as solvents. Methanol (Univar, Ar grade) was used in the methanol permeation study. Zeolite Y (Si/Al ratio = 5.1; Zeolyte International) and graphene oxide (Top New Energy Co., Ltd.) were used as fillers in S-PSF membrane.

4.3.2 Preparation of Sulfonated Graphene Oxide (S-GO)

50 mg of graphene oxide was added to 8 ml of 0.06 M sulfanilic acid solution at 70 °C. Under continuous stirring, 2 ml of 0.006 M sodium nitrite solution was added drop wise and held at 70 °C for 12 h. After reaction, the mixture was collected by filtration and washed with deionized water several times until the pH became neutral. The S-GO was then dried at 70 °C for 24 h (Chien *et al.*, 2013).

4.3.3 Preparation of Sulfonated Polysulfone (S-PSF)

The polymer solution was prepared by dissolving PSF (2 g) in a 10 mL of DCM. The concentrated H_2SO_4 (98%) was added into the polymer solution at an acid:polymer mole ratio of 80 at room temperatures. The sulfonated solution was continuously stirred for 4 h, and then the solution was precipitated by methanol in an ice bath. The precipitate was washed by DI water until pH of precipitate reached neutral. The S-PSF was dried at 100 °C for 24 h (Macksasitorn *et al.*, 2012).

4.3.4 Composite Membrane Preparation

1 g of S-PSF was dissolved in a 12 mL of DMAc to prepare a polymer solution. The polymer solution was continuously stirred until homogenous. The zeolite Y (5, 10, 15, and 20 %v/v) and S-GO (1, 2, 3, 5, and 7%v/v) were added into the polymer solution and stirred continuously for 24 h. The film was formed by a solution casting technique and heated at 70 °C for 24 h under a vacuum.

4.3.5 Characterizations of S-PSF and S-GO

The functional groups of S-PSF and S-GO were determined using the Fourier transform infrared spectroscopy (Nicolet, Nexus 670 FT-IR spectrometer). The samples, used in powder form, were grinded and mixed with potassium bromide as background, and compressed into pellets (Macksasitorn *et al.*, 2012). The measurements were carried out in the in the wavenumber range of 1600-400 cm^{-1} with 64 scans.

The structures of S-PSF were determined by the nuclear magnetic resonance spectroscopy (Bruker Biospin Avance 500 MHz NMR spectrometer) using

deuterated dimethyl sulfoxide (DMSO-d_6) as the solvent and the experiment was conducted at room temperature.

X-ray photoelectron spectroscopy (XPS) was used for the determination of surface composition of the GO and S-GO. The surface morphology of GO and S-GO was investigated using the scanning electron microscopy (SEM).

4.3.6 Characterizations of Composite Membranes

4.3.6.1 Thermal Stability

The thermal property of S-PSF and composite membranes was investigated using a Thermo-Gravimetric/Differential Thermal Analyzer (TG/DTA; Perkin Elmer, Pyris Diamond). The samples were weighed in the range of 4-10 mg and inserted into alumina pans. The measurements were carried out under nitrogen flow between 30 to 700 °C at a heating rate of 10 °C min^{-1} (Zhang *et al.*, 2011).

4.3.6.2 Water Uptake

In the water uptake measurement, the membranes were immersed into deionized water for 24 h at room temperature. Excess water was removed from the membrane surface with a paper and the membrane was weighed (noted as W_s). The membranes were dried at 100 °C for 24 h in a vacuum oven and weighed (noted as W_d). The percentage of water uptake was then calculated as in the following Eq. (4.1).

$$\text{Water uptake (\%)} = \frac{(W_s - W_d)}{W_d} \times 100 \qquad (4.1)$$

4.3.6.3 Proton Conductivity (σ)

Proton conductivity of the membranes was measured by an impedance phase analyzer (HP, model 4194) under dry state and under wet state at frequencies from 100 Hz to 2 MHz and at room temperature. The membranes were cut into a 5 × 5 cm^2 specimen for the measurement with and without immersing in deionized water at room temperature for 24 h before measurement. Proton conductivity was calculated as in the following Eq. (4.2):

$$\sigma\ (\mathrm{S/cm}) = \frac{d}{R \times A} \qquad (4.2)$$

where σ is the proton conductivity (S cm^{-1}), d is the thickness of the membrane (cm), A is the area of the interface of membrane in contact with the electrodes (cm^2), and R refers to the measured resistance of the membrane derived from the high frequency semi-circle on the complex impedance plane with the Z axis (ohm) (Ahmad *et al.*, 2006).

4.3.6.4 Methanol Permeability (P)

The methanol permeability refers the amount of methanol that permeates through the membrane. The permeation cell for methanol permeability measurement consisted of chamber A and chamber B as separated by the polymer membrane. Chamber A was filled with 250 ml of methanol solution (2.0 M). Chamber B was filled with 250 ml of DI water. The membrane was placed between chamber A and chamber B. The methanol permeability was calculated as in the following Eq. (4.3):

$$P\ (\mathrm{cm^2/s}) = \frac{k_B \times V_B \times L}{A \times (C_A - C_B)} \qquad (4.3)$$

where P is the methanol permeability, C_A and C_B are the methanol concentrations in the compartments A and B respectively, A and L are the area and the thickness of a membrane respectively, V_B is the volume of the solution in the compartment B, k_B is the slope of the methanol concentration profile in the compartment B. The methanol concentrations were measured with a thermal conductivity detector (TCD) in gas chromatography (GC; Agilent, 7820A) where ethanol was used as the internal standard (Zhai *et al.*, 2007).

The overall membrane performance was evaluated by selectivity defined as the ratio of proton conductivity to methanol permeability. The higher selectivity of

the membrane is better, because the membrane can act as both a good conductor and a good separator for DMFC.

4.3.6.5 Mechanical Properties

The mechanical properties namely the tensile strength, yield strain, and Young's modulus were measured using a universal testing machine (Lloyd, model SMT2-500N) at room temperature with a 25 $mm.min^{-1}$ speed. The membranes with 200 μm thick were cut into 1 × 5 cm^2 specimens. Each sample was measured from 5 specimens and the average value was taken.

4.4 Results and Discussion

4.4.1 Characterizations of S-PSF

4.4.1.1 Fourier Transform Infrared Spectroscopy (FT-IR)

FTIR spectroscopy was used to identify the characteristic peaks corresponding to the sulfonic acid groups ($-SO_3H$) in polymeric structure. The FTIR spectra of PSF and S-PSF are in wavenumber range of 1500 to 600 cm^{-1} as shown in Figure 4.1 and identified as PSF and S-PSF72 spectra, respectively. The characteristic peaks at 1010 and 1078 cm^{-1} as observed in the sulfonated polymer can be assigned to the symmetric and asymmetric stretchings of $-SO_3H$ groups, respectively. Furthermore, these two peaks become broader with increasing DS (Devrim *et al.*, 2009). Additionally, the symmetric and asymmetric stretchings of O=S=O are also observed at 1147 cm^{-1} (Devrim *et al.*, 2009) and 1244 cm^{-1} (Karlsson *et al.*, 2004).

4.4.1.2 Nuclear Magnetic Resonance (^{1}H-NMR)

Figure 4.2 shows the ^{1}H-NMR spectrum of S-PSF to confirm the successful sulfonation. The proton resonance at 7.80 ppm is assigned to the proton adjacent to the new pendant of $-SO_3H$ groups (Devrim *et al.*, 2009 and Unnikrishnan *et al.*, 2012). Therefore, the FT-IR and ^{1}H-NMR spectrum verify the presence of $-SO_3H$ groups in the PSF backbone after the sulfonation reaction.

4.4.1.3 Thermogravimatric Analysis (TGA)

The PSF exhibits excellent thermal stability with a single step degradation at temperature higher than 500 °C as shown in Figure 4.3. The S-PSF thermogram obviously demonstrates three-step degradation. In the first step, the weight loss between 50 and 180 °C can be related to loss of water and residual solvent during casting. The second step weight loss, between 180 and 400°C, can be attributed to the decomposition of $-SO_3H$ groups. The third thermal degradation is the degradation of the polymer backbone, which occurs around 450 °C and is lower than that of pristine PSF, because the sulfonic acid groups aids in the degradation of the PSF backbone (Unnikrishnan *et al.*, 2012).

4.4.2 Characterizations of S-GO

4.4.2.1 Fourier Transform Infrared Spectroscopy (FT-IR)

The results of FT-IR analysis indicate the differences between the GO and S-GO spectra. In Figure 4.4, both GO and S-GO spectra show the characteristic peaks at 1054 and 1720 cm^{-1} corresponding to the C-O stretching and C=O carbonyl stretching, respectively (Zhang *et al.*, 2013). In the spectrum of S-GO, a new peak appears at 1277 cm^{-1}, which indicates the typical absorbance of the $-SO_3H$ groups (Heo *et al.*, 2012). Moreover, the $\nu_{S\text{-phenyl}}$ and $\nu_{S\text{-}O}$ vibration are observed at 1036 and 1127, 1164 cm^{-1}. The other new peak at 3431 cm^{-1} can be clearly assigned to the O-H stretching after sulfonation (Zhang *et al.*, 2013).

4.4.2.2 X-Ray Photoelectron Spectroscopy (XPS)

The XPS spectra of GO and S-GO are shown in Figure 4.5. The wide scan spectra in the range of 0-1200 eV are used to identify the surface elements. In both GO and S-GO spectra, C 1s and O 1s signals appear at 286 and 531 eV, respectively. S-GO shows a new S 2p peak at 168 eV after functionalizing with the sulfonic acid groups onto GO (Heo *et al.*, 2012). The O 1s spectra of S-GO slightly increases compared to that of GO because of the sulfonic groups in S-GO. The XPS spectra show clear evidence that the GO was chemically modified, as confirmed by high resolution spectra of S 2p and C 1s based on spectral deconvolution. The S 2p peak at 168 eV is attributed to the binding energy of

sulfonic groups (Chien *et al.*, 2013), as shown in Figure 4.5(d). The C 1s peaks of GO (Figure 4.5(e)) appearing at 283.5, 284.3, 285.9, 286.9, 288.4 and 290.1 eV, represent the C=C, C-C/C-H, C-OH, C-O-C, C=O and O-C=O, respectively. The C 1s spectra of the S-GO (Figure 4.5(f)) are different when compared to GO, it insignificantly decreases after the sulfonated reaction. The C-S bond is contributed to the peak observed at 283.9 eV (Zarrin *et al.*, 2011). These results confirmed the successful introduction of the sulfonic acid groups on the surface of GO.

The degree of substitution (DS) of sulfonic acid groups in GO was quantitatively determined by comparing the O 1s peak of GO with that of S-GO (Shim *et al.*, 2012). So, the DS of S-GO is 63.84 % and the percentage yield of S-GO was approximately 80.

4.4.2.3 Scanning Electron Microscopy (SEM)

Surface morphology of the (a) GO and (b) S-GO were observed by SEM as shown in Figure 4.6. A comparison of morphology of GO with S-GO reveals that the surface of the S-GO is rougher than that of the GO because of the sulfonation process (Heo *et al.*, 2012). Therefore, the FT-IR, XPS and SEM confirm the presence of $-SO_3H$ groups in the GO after the sulfonation reaction.

4.4.3 Characterization of Composite Membranes

4.4.3.1 Thermal Stability

The thermograms of S-PSF and S-PSF/Zeolite Y composite membranes are shown in Figure 4.7. Both TGA thermograms of composite membranes show three steps degradations. The degradation behavior and mechanism of S-PSF remain unchanged after incorporating the filler. In the first step, the weight loss between 50 and 250 °C, can be related to losses of water and residual solvent during casting. In the second step, between 250 and 430 °C, the weight loss can be attributed to the decomposition of sulfonic acid groups. The third thermal degradation is the degradation of the polymer backbone, which occurs around 500 °C. Zeolite Y particles slightly enhance the thermal stability of S-PSF membrane by increasing crystallinity of polymer matrix (Devrim *et al.*, 2009).

The TGA thermograms of the S-PSF/S-GO membranes are shown in Figure 4.8. All membranes undergo the following three steps degradation. In the first step, the weight loss between 50 and 230 °C, can be related to losses of water and residual solvent during casting. In the second step, between 230 and 400 °C, the weight loss can be attributed to the decomposition of sulfonic acid groups. The third thermal degradation is the degradation of the polymer backbone, which also occurs around 500 °C. The TGA thermograms of S-PSF/S-GO membranes are retarded at the second and third stages compared with the pristine S-PSF which have higher onset temperatures at these two stages. The S-PSF membrane with 7% v/v of S-GO loading shows a lower temperature in the second step but a higher temperature in the third step. These results suggest that the interaction between S-GO and S-PSF should be contributed to delay the degradation of S-PSF chains leading to an increase in the degradation temperatures (Liu *et al.*, 2014).

Therefore, the fillers enhance the thermal stability of composite membrane, as shown in Figure 4.7 and 4.8. TGA results imply that the composite membranes are thermally stable at temperatures below 200 °C, adequate for the application in DMFC.

4.4.3.2 Water Uptake

The water uptake in a membrane generally dictates the hydrophilic nature of polymer (Unnikrishnan *et al.*, 2012) and directly relates to the proton conductivity of the membrane (Auimviriyavat *et al.*, 2011). The water uptake values of S-PSF and S-PSF/Zeolite Y membranes are shown in Figure 4.9. The water uptake of S-PSF/Zeolite Y membranes increases with increasing zeolite Y content and are higher than that of pristine S-PSF. This is possibly due to the unique pore size and hygroscopic property of zeolite Y, which creates a sufficient number of water channels and affects the proton motion (Unnikrishnan *et al.*, 2012). As shown in Table 4.1, the water uptake of the S-PSF is 9.01 ± 0.57 %, while the water uptakes of S-PSF, S-PSF/5Y, S-PSF/10Y, S-PSF/15Y, and S-PSF/20Y are 15.01 ± 0.86 %, 15.35 ± 1.03%, 20.88 and 22.07 ± 0.44 %, respectively.

The water uptakes of S-PSF/S-GO membranes are shown in Figure 4.10. The S-PSF/S-GO membranes show a decreasing tendency in water

uptake with increasing S-GO content. The S-PSF membranes with a S-GO content below 3% v/v exhibit the increasing value of water uptake when compared with pristine S-PSF membrane owing to the small amount of fillers and the functional groups of fillers, creating the temporary water adsorption channels in membranes. Above 3% v/v of S-GO, the blocking effect becomes dominant. The large amount and large aspect ratio of S-GO can act as barriers to water adsorption, thus reducing the water uptake of the membranes (Heo *et al.*, 2012). Another reason is the increase in interfacial interaction between hydrogen bonds of S-GO and S-PSF, leading to the decrease in the ionic channel size where the water molecules pass through. Therefore, the decrease in ionic channel size effectively prevents the adsorption of water molecules (Chien *et al.*, 2013).

4.4.3.3 Proton Conductivity

The proton conductivity of S-PSF and S-PSF/Zeolite Y membranes was measured under a wet state at 27 °C. The proton conductivity increases after the sulfonation reaction because the $-SO_3H$ groups provide more hydrophilic pathways for proton transport through the membrane (Auimviriyavat *et al.*, 2011). Nevertheless, the proton conductivity of S-PSF membrane, which is in the range of 10^{-3} - 10^{-4} $S.cm^{-1}$ under wet state, is still lower than that of Nafion 117 (under wet state), which is 3.17×10^{-3} $S.cm^{-1}$. The addition of zeolite Y is expected to enhance the proton conductivity of S-PSF membranes compared to that of the pristine S-PSF membrane. For the effect of zeolite Y content, the proton conductivity increases with increasing the zeolite Y content as shown in Figure 4.11 because zeolite Y creates $-SO_3H$ conductivity sites within the membrane matrix and enhances the motion of the protons by its water retention characteristics (Devrim *et al.*, 2009). In Table 4.1, the highest proton conductivity of 2.33×10^{-3} $S.cm^{-1}$ belongs to the S-PSF membrane with the zeolite Y content of 15 %v/v. However, the proton conductivity of S-PSF/20Y is relatively lower because the large amount of zeolite loading leads to a poorer distribution of zeolite particles in polymer matrix and reduces proton conductivity (Auimviriyavat *et al.*, 2011).

Figure 4.12 shows the proton conductivities of S-PSF/S-GO membranes. The proton conductivity of S-PSF/S-GO membranes shows an

increasing tendency with the increase in S-GO loading (up to 4.27×10^{-3} $S.cm^{-1}$ at 3% v/v). The incorporation of S-GO in S-PSF membranes leads to an increase in the sulfonic acid groups which form the interconnected ionic clusters where protons can transport quickly (Chien *et al.*, 2013, Nicotera *et al.*, 2011). On the contrary, the proton conductivity decreases at S-GO loading above 3% v/v. The blocking effect starts to dominate here where S-GO particles obstruct polymer chains in the ionic clusters thus decreasing the proton conductivity (Heo *et al.*, 2012). Hence, the loading of S-GO of approximately 3%v/v is suitable to improve proton transport in the S-PSF/S-GO membranes.

4.4.3.4 Methanol Permeability and Selectivity

The methanol permeability measurement is one of basic tests for DMFC because permeability is the cause for the loss of fuel and the decrease in efficiency (Vernersson *et al.*, 2006). Methanol molecules can transport with the electro-osmotic drag in DMFC due to methanol properties (Carrette *et al.*, 2001). In this work, the methanol permeability value cannot be collected at room temperature. So, the measurement temperature was raised up to 70 °C to provide an ease in methanol permeability. Table 4.1 shows the methanol permeability values of Nafion117 and composite membranes. The effect of zeolite Y content within the S-PSF membranes was investigated. They possess the methanol permeability values of 1.10×10^{-6}, 1.30×10^{-6}, 1.59×10^{-6}, and 1.64×10^{-6} $cm^2.s^{-1}$, for zeolite Y contents of 5, 10, 15, and 20 %v/v, respectively. It seem that the methanol permeability increases with an increment in zeolite Y due the hygroscopic property and unique pore size of zeolite Y which can adsorb methanol towards the pore and pass it through another side (Wang *et al.*, 2008). It seems reasonable to suppose that the increasing of the water uptake of membranes would also have effect on the permeability. Expectedly, the methanol permeability value of all composite membranes is still lower than that of the pristine S-PSF and Nafion 117. Moreover, the selectivities of all S-PSF/Zeolite Y membranes are of higher values than that of Nafion117. The highest selectivity of 1.65×10^{-3} $s.S.cm^{-3}$ belongs to the zeolite Y loading of 15%v/v.

In case of the S-PSF/S-GO membranes, the methanol permeability shows a decreasing tendency because of the blocking effect of S-GO

particles and the interfacial interaction between S-GO and S-PSF. The S-GO particles in S-PSF membrane act as the barriers and obstruct the methanol transporting through the membranes. The transportation of methanol in the membranes requires broad ionic channels but the strong interfacial interaction limits the ionic channel size, leading to a decrease in methanol permeability (Heo *et al.*, 2012). The selectivity of the pristine S-PSF is significantly improved and exhibits much better performance when compared to Nafion117 membrane. The maximum selectivity occurs at 3% v/v of S-GO loading and is approximately 100 times that of Nafion 117. Therefore, S-PSF/S-GO membranes are absolutely promising membranes for DMFC applications.

4.4.3.5 Mechanical Properties

The mechanical properties of all composite membranes at room temperature (27 °C) are shown in Table 4.2. The tensile strength, elongation at break, and Young's modulus of all composite membranes were measured and evaluated. For the S-PSF/zeolite Y composite membranes, the tensile strengths at 5, 10, 15, and 20% v/v loadings are 26.1, 25.5, 15.7, and 21.4 MPa, respectively. It is possible that the interfacial interaction between the S-PSF matrix and zeolite Y is not strong enough, causing a loss of strength. The elongations at break of the composite membranes at 5, 10, 15, and 20% v/v loadings are 4.3, 4.5, 3.4, and 2.7 %, respectively. While the Young's modulus values of the composite membranes at 5, 10, 15, and 20% v/v loadings are 1011, 1212, 1208, and 3205 MPa, respectively. These values are much higher than that of the S-PSF and Nafion117 membranes. Unfortunately, the S-PSF composite membrane with 20% v/v of zeolite Y content becomes a brittle material because of the presence of zeolite particles in S-PSF matrix leading to a restriction on the chain stretching and a limitation on its use for PEMs.

The addition of S-GO obviously influences the mechanical properties of the S-PSF/S-GO membranes. From Table 4.2, the incorporations of 1, 2, 3, 5, and 7% v/v elevate the tensile strength to 29.4, 36.5, 40.1, 44.0 and 48.9 MPa, along with the young's modulus of 873, 907, 947, 1050 and 1187 MPa, respectively. The mechanical properties show improving trends with increasing

S-GO. The enhanced mechanical properties can be reasonably described by the interfacial interaction between S-GO and S-PSF which inhibits the chain mobility (Liu *et al.*, 2014). On the other hand, the elongation at break of the S-PSF/S-GO membranes at 1, 2, 3, 5, and 7% v/v are 5.4, 4.4, 3.4, 2.8 and 2.6 %, respectively. This decreasing trend might be due to the restriction of the polymer chains by S-GO particles, making the membrane became more brittle.

4.4.4 Hybrid Membranes

The best performance of each system was selected to prepare the hybrid membranes, consisting of S-PSF membrane with both S-GO and zeolite Y. The variation of zeolite Y concentration (12 and 15% v/v) was investigated while S-GO concentration was fixed (3% v/v). The results are shown in Table 4.1. It can be observed that the proton conductivity and methanol permeability are of values as zeolite Y content increases. The increase in zeolite Y content causes the agglomeration of zeolite Y particles as well as the zeolite Y particles interfere with the interaction between S-GO with S-PSF by its smaller molecules; these factors resist water and methanol molecules to pass through the membrane. These results are consistent with the decrease in the water uptake value. For their selectivity, they show lower selectivity values. Nevertheless, the hybrid membrane exhibits superior performance when compared with the pristine S-PSF and Nafion117 membranes.

The mechanical properties of hybrid membrane were also investigated as shown in Table 4.2. The tensile strength is significantly dropped from 40 MPa to 14.9 and 13.5 MPa after adding the zeolite Y at 12 and 15% v/v, respectively. This suggests that the incorporation of zeolite Y in S-PSF/S-GO membrane probably impede the interaction between S-GO and S-PSF resulting in a poorer interaction. The elongations at break of the hybrid membranes are 2.3, and 2.0 %, while the Young's modulus values are 1209, and 1389 MPa, respectively. Unexpectedly, both hybrid membranes show poorer mechanical properties and become brittle materials because of the reduction in elongation at break. So the hybrid membranes might not be suitable as PEM, although the hybrid membranes demonstrate good performances for DMFC applications.

4.5 Conclusions

The S-PSF was prepared by a mild sulfonation method. The FT-IR and NMR results showed the successful attaching of sulfonic acid groups onto PSF backbone. The XPS and SEM results also confirmed the functionalized GO by sulfonation. The effects of zeolite Y and S-GO on the performance of composite membranes were investigated; the series of PEMs were prepared by incorporation of filler into S-PSF. For the effect of zeolite Y content, the proton conductivity increased with increasing zeolite Y content. However, the methanol permeability increased with increasing zeolite Y due to its hygroscopic property. For the composite membranes based on S-PSF with S-GO, the incorporation of S-GO particles improved the proton conductivity of S-PSF membranes up to 4.27×10^{-3} $S.cm^{-1}$, which can be attributed to the increase in the sulfonic acid groups of S-GO forming interconnected ionic clusters for proton migration. The S-GO particles positively influenced and efficiently blocked water and methanol molecules, leading to the decreases in the water uptake and methanol permeability. The hybrid membranes were investigated for further improvement. They showed lower performances when compared with S-PSF/S-GO (3%v/v) membranes but still showed better performances than Nafion117 membrane. Consequently, the selectivity of all composite membranes exhibited a superior performance relative to the Nafion117 membrane. It can be concluded that the fabricated composite membrane (3%v/v S-GO) is the most promising material for use as a PEM in DMFC applications.

4.6 Acknowledgements

The authors would like to acknowledge the financial supports from Conductive and Electroactive Polymers Research Unit of Chulalongkorn University, The Thailand Research Fund (TRF), and the Royal Thai Government.

4.7 References

Ahmad, H., Kamarudin, S.K., Hasran, U.A., and Daud, W.R.W. (2010) Overview of hybrid membranes for direct-methanol fuel-cell applications. International Journal of Hydrogen Energy, 35(5), 2160-2175.

Ahmad, M.I., Zaidi, S.M.J., and Rahman, S.U., (2006) Proton conductivity and characterization of novel composite membranes for medium-temperature fuel cells. Desalination, 193(1–3), 387-397.

Auimviriyavat, J., Changkhamchom, S., and Sirivat, A. (2011) Development of poly(ether ether ketone) (PEEK) with inorganic filler for direct methanol fuel cells (DMFCs). Industrial & Engineering Chemistry Research, 50(22), 12527-12533.

Carrette, L., Friedrich, K.A., and Stimming, U. (2001) Fuel Cells – Fundamentals and Applications. Fuel Cells, 1(1), 5-39.

Chen, S., Yin, Y., Kita, H., and Okamoto, K.-I. (2007) Synthesis and properties of sulfonated polyimides from homologous sulfonated diamines bearing bis(aminophenoxyphenyl) sulfone. Journal of Polymer Science Part A: Polymer Chemistry, 45(13), 2797-2811.

Chien, H.-C., Tsai, L.-D., Huang, C.-P., Kang, C.-Y., Lin, J.-N., and Chang, F.-C. (2013) Sulfonated graphene oxide/Nafion composite membranes for high-performance direct methanol fuel cells. International Journal of Hydrogen Energy, 38(31), 13792-13801.

Devrim, Y., Erkan, S., Baç, N., and Eroğlu, I. (2009) Preparation and characterization of sulfonated polysulfone/titanium dioxide composite membranes for proton exchange membrane fuel cells. International Journal of Hydrogen Energy, 34(8), 3467-3475.

Gao, Y., Robertson, G. P., Guiver, M. D., Jian, X., Mikhailenko, S. D., Wang K., and Kaliaguine S. (2005) Sulfonation of poly(phthalazinones) with fuming sulfuric acid mixtures for proton exchange membrane materials. Journal of Membrane Science, 227(1-2), 39-50.

Ghassemi, H. and McGrath, J.E. (2004) Synthesis and properties of new sulfonated poly(p-phenylene) derivatives for proton exchange membranes. Polymer, 45, 5847-54.

Heo, Y., Im, H., and Kim, J. (2013) The effect of sulfonated graphene oxide on Sulfonated Poly (Ether Ether Ketone) membrane for direct methanol fuel cells. Journal of Membrane Science, 425-426, 11-22.

Karlsson, L.E. and Jannasch P. (2004) Polysulfone ionomers for proton-conducting fuel cell membranes: sulfoalkylated polysulfones. Journal of Membrane Science, 230(1–2), 61-70.

Kobayashi, T., Rikukawa, M., Sanui, K., and Ogata, N. (1998) Proton-conducting polymers derived from poly(ether-etherketone) and poly(4-phenoxybenzoyl-1, 4-phenylene). Solid, 106, 219-225.

Liu, F., Ma, B.R., Zhou, D., Xiang, Y.H., and Xue, L.X. (2014) Breaking through tradeoff of Polysulfone ultrafiltration membranes by zeolite 4A. Microporous and Mesoporous Materials, 186, 113-120.

Lufrano, F., Baglio, V., Staiti, P., Arico, A.S., and Antonucci, V. (2006) Development and characterization of sulfonated polysulfone membranes for direct methanol fuel cells. Desalination, 199(1-3), 283-285.

Lufrano, F., Baglio, V., Staiti, P., Arico, A.S., and Antonucci, V. (2008) Polymer electrolytes based on sulfonated polysulfone for direct methanol fuel cells. Journal of Power Sources, 179(1), 34-41.

Macksasitorn, S., Changkhamchom, S., Sirivat, A., and Siemanond, K. (2012) Sulfonated poly(ether ether ketone) and sulfonated poly(1,4-phenylene ether ether sulfone) membranes for vanadium redox flow batteries. High Performance Polymers, 24(7), 603-608.

Miyatake, K., Yasuda, T., Hirai, M., Nanasawa, M., and Watanabe, M. (2007) Synthesis and properties of a polyimide containing pendant sulfophenoxypropoxy groups. Journal of Polymer Science Part A: Polymer Chemistry, 45(1), 157-163.

Nicotera, I., Simari, C., Coppola, L., Zygouri, P., Gournis, D., Brutti, S., and Baglio, V. (2011) Sulfonated graphene oxide platelets in nafion nanocomposite

membrane: advantages for application in direct methanol fuel cells. The Journal of Physical Chemistry C, 118(42), 24357-24368.

Qiao, J., Hamaya, T., and Okada, T. (2005) New highly proton-conducting membrane poly(vinylpyrrolidone) (PVP) modified poly(vinyl alcohol)/2-acrylamido-2-methyl-1- propanesulfonic acid (PVA–PAMPS) for low temperature direct methanol fuel cells (DMFCs). Polymer, 46, 10809-10816.

Shim, S. H., Kim, K. T., Lee, J. U., and Jo, W. H. (2012) Facile method to functionalize graphene oxide and its application to poly(ethylene terephthalate)/graphene composite. ACS Applied Materials and Interfaces, 4(8), 4184-4191.

Unnikrishnan, L., Madamana, P., Mohanty, S., and Nayak, S.K. (2012) Polysulfone/C30B nanocomposite membranes for fuel cell Applications: Effect of various sulfonating agents. Polymer-Plastics Technology and Engineering, 51(6), 568-577.

Vernersson, T., Lafitte, B., Lindbergh, G., and Jannasch, P. (2006) A Sulfophenylated Polysulfone as the DMFC Electrolyte Membrane – an Evaluation of Methanol Permeability and Cell Performance. Fuel Cells, 6(5), 340-346.

Wang, F., Hickner, M., Qing, J., Harrison, W., Mecham, J., Zawodzinski, T.A. and McGrath, J.E. (2001) Synthesis of highly sulfonated poly(arylene ether sulfone) random (statistical) copolymers via direct polymerization, Macromolecules, 175, 387-395

Wang, J., Zheng, X., Wu, H., Zheng, B., Jiang, Z., Hao, X., and Wang, B. (2008) Effect of zeolites on chitosan/zeolite hybrid membranes for direct methanol fuel cell. Journal of Power Sources, 178(1), 9-19.

Wootthikanokkhan, J. and Seeponkai, N. (2006) Methanol permeability and properties of DMFC membranes based on sulfonated PEEK/PVDF blends. Journal of Applied Polymer Science, 102(6), 5941-5947.

Yildirim, M.H., Curòs, A.R., Motuzas, J., Julbe, A., Stamatialis, D.F., and Wessling M. (2009) Nafion®/H-ZSM-5 composite membranes with superior

performance for direct methanol fuel cells. Journal of Membrane Science, 338(1–2), 75-83.

Zarrin, H., Higgins, D., Jun, Y., Chen, Z., and Fowler, M. (2011) Functionalized graphene oxide nanocomposite membrane for low humidity and high temperature proton exchange membrane fuel cells. The Journal of Physical Chemistry C, 115(42), 20774-20781.

Zhang, Z., Desilets, F., Felice, V., Mecheri, B., Licoccia, S., and Tavares, A.C. (2011) On the proton conductivity of Nafion–Faujasite composite membranes for low temperature direct methanol fuel cells. Journal of Power Sources, 196(22), 9176–9187.

Zhang, L., Shi, T., Wu, S., and Zhou, H. (2013) Sulfonated graphene oxide: the new and effective material for synthesis of polystyrene-based nanocomposites. Colloid and Polymer Science, 291(9), 2061-2068.

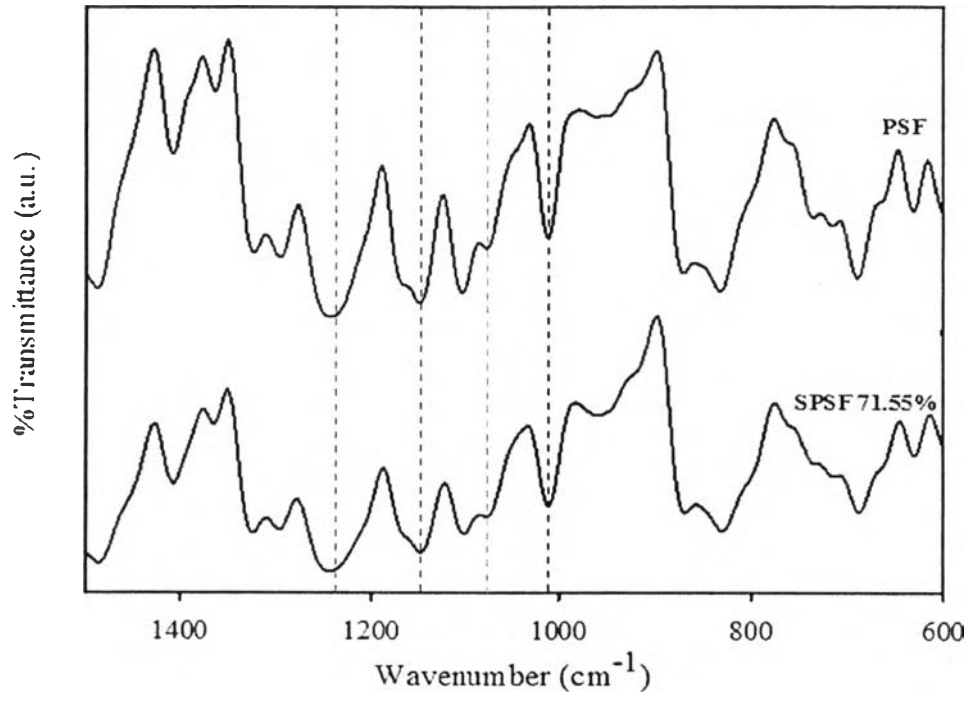

Figure 4.1 FT-IR spectra of PSF and S-PSF72.

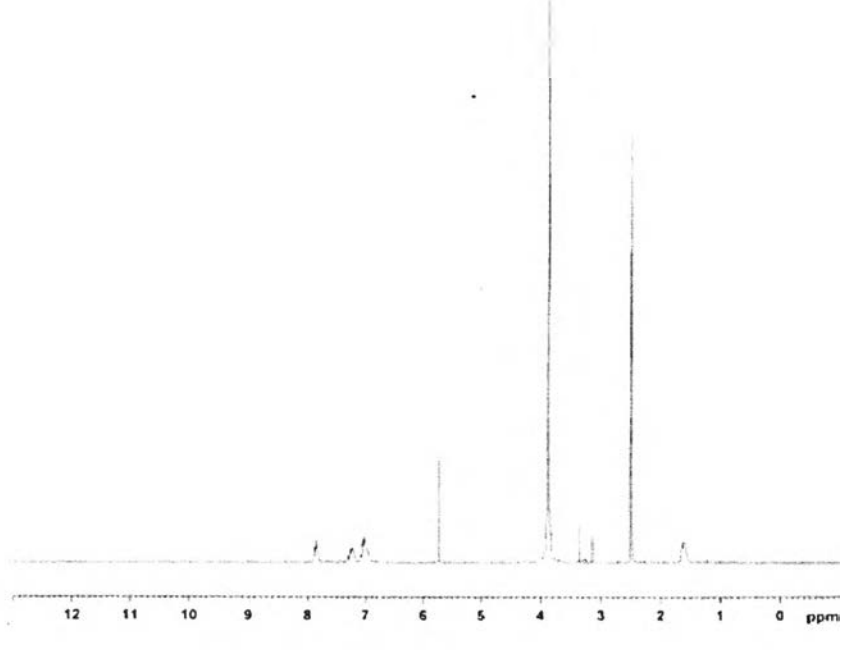

Figure 4.2 ^{1}H-NMR spectrum for S-PSF72.

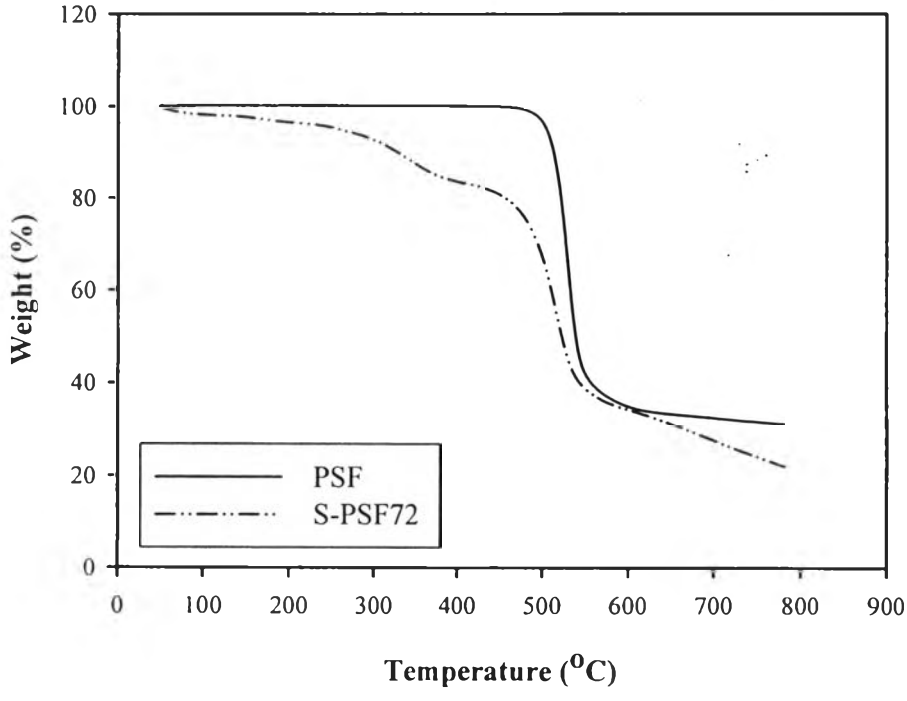

Figure 4.3 TGA thermograms of PSF and S-PSF72.

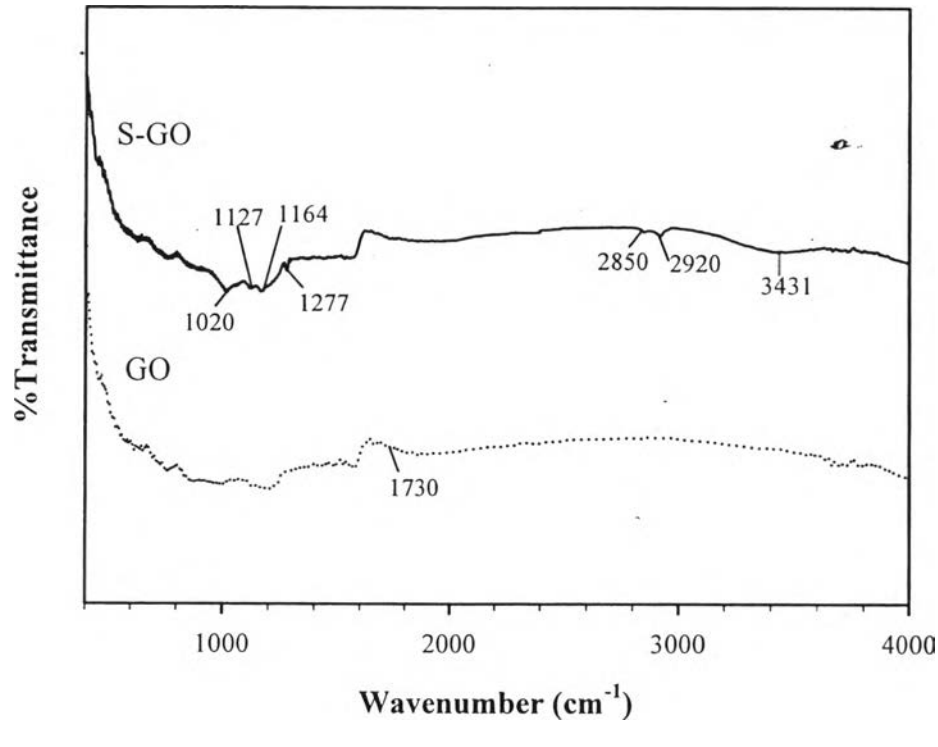

Figure 4.4 FTIR spectra of GO and S-GO.

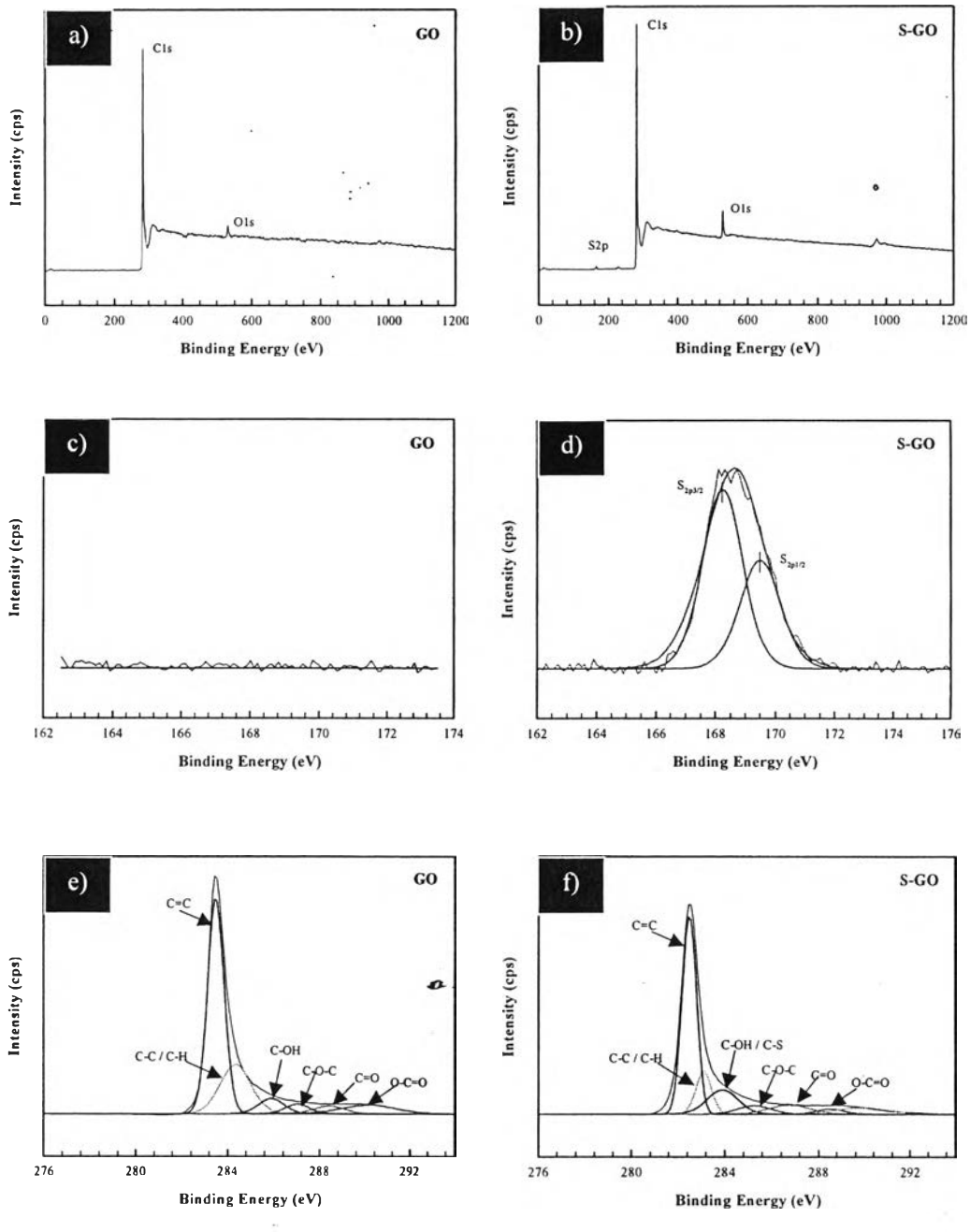

Figure 4.5 Wide region XPS spectra of: (a) GO, (b) S-GO, (c) S2p spectra of GO, (d) S2p spectra of S-GO, (e) C1s spectra of GO and (f) C1s spectra of S-GO.

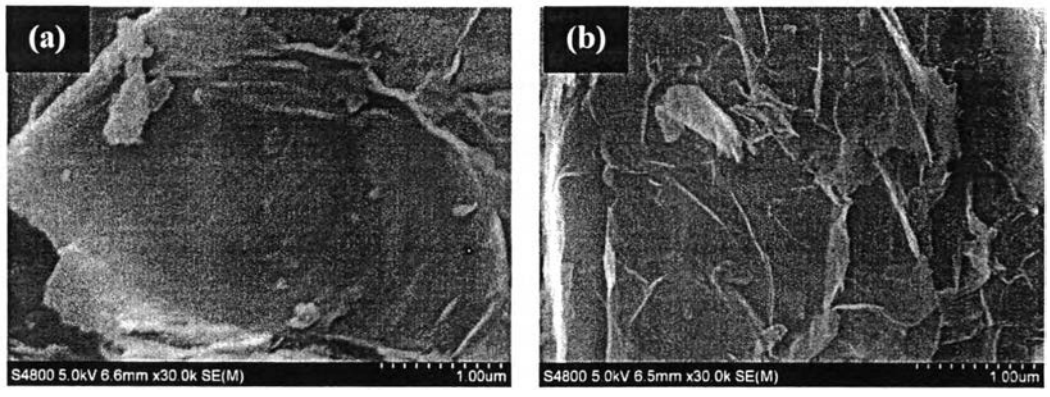

Figure 4.6 SEM images of the surface of: (a) GO and (b) S-GO.

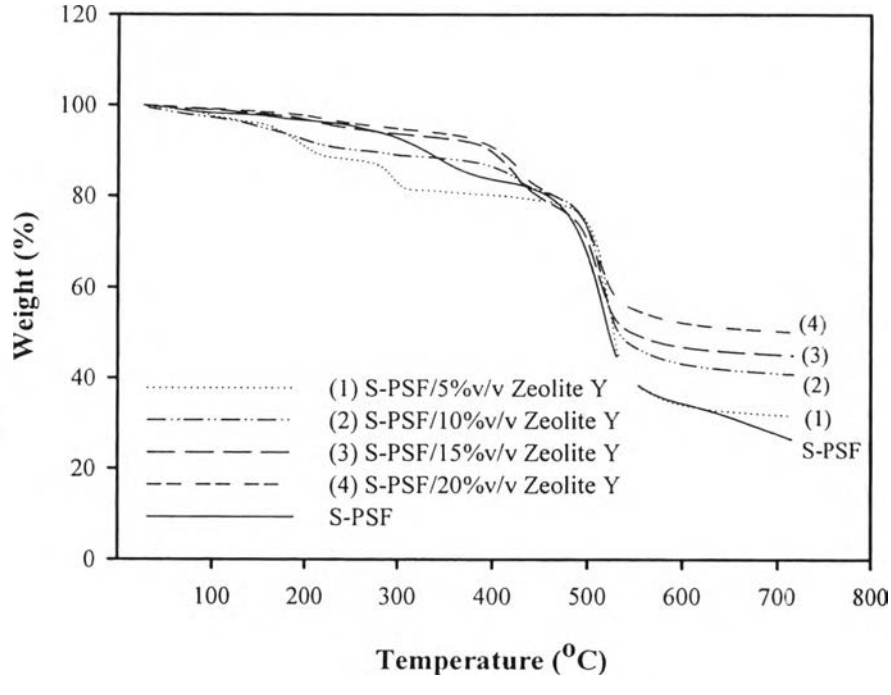

Figure 4.7 TGA thermograms for S-PSF/Zeolite Y composite membranes.

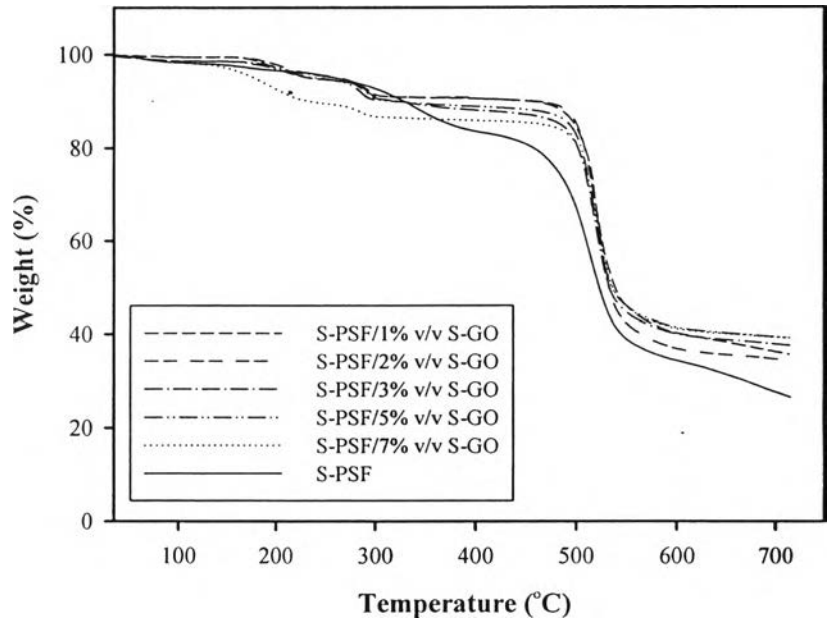

Figure 4.8 TGA thermograms for S-PSF/S-GO composite membranes.

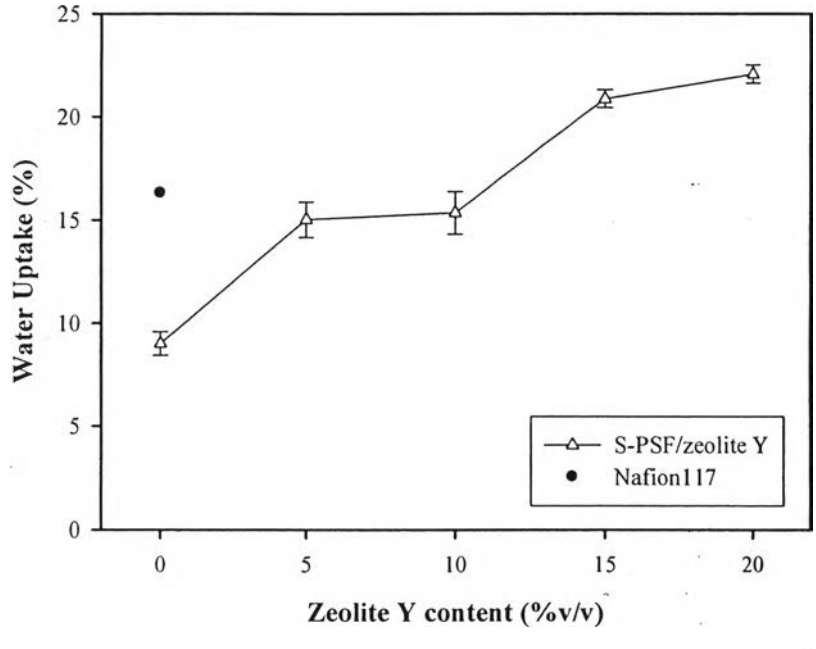

Figure 4.9 Water uptake (%) for S-PSF and S-PSF/Zeolite Y composite membranes.

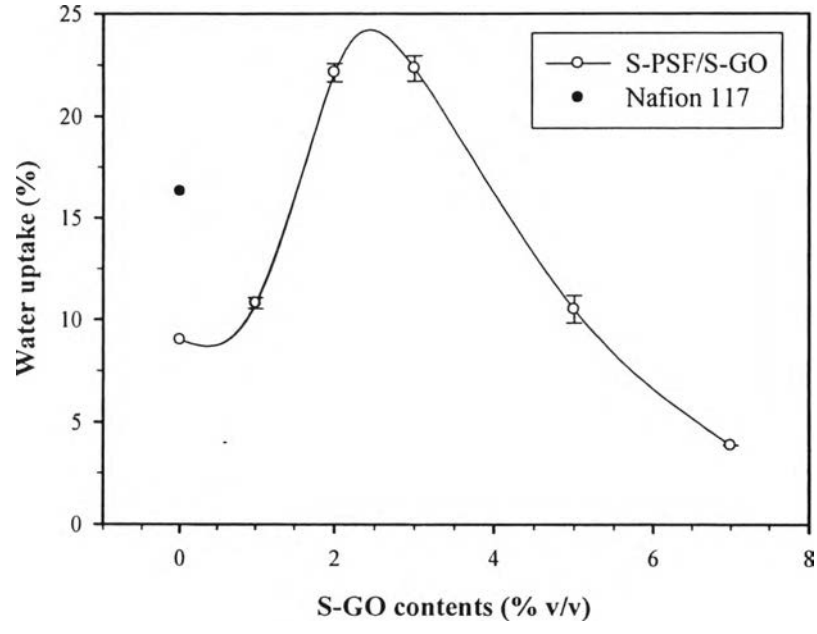

Figure 4.10 Water uptake (%) for S-PSF and S-PSF/S-GO composite membranes.

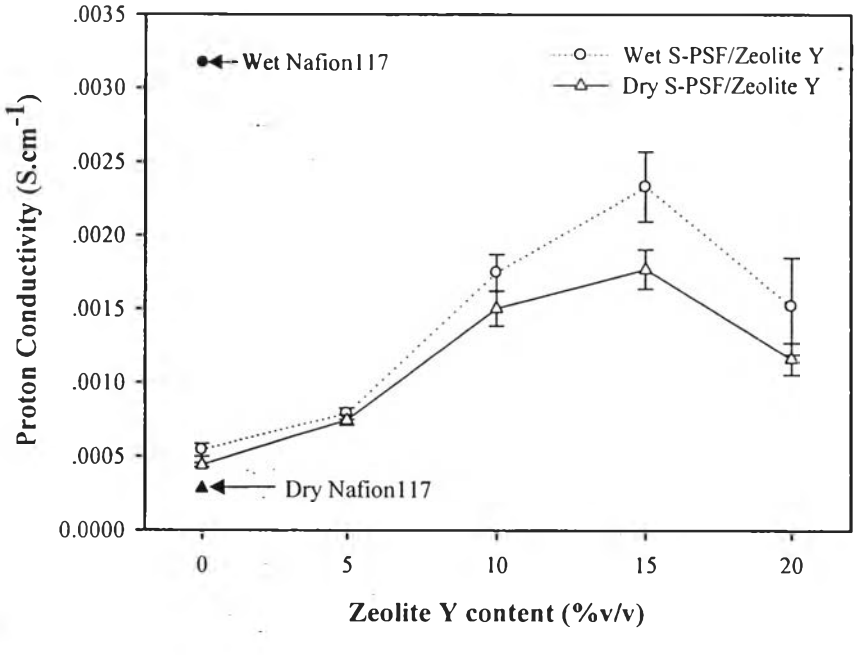

Figure 4.11 Proton conductivity of the S-PSF/Zeolite Y composite membranes with a DS of 0.72 at 27 °C.

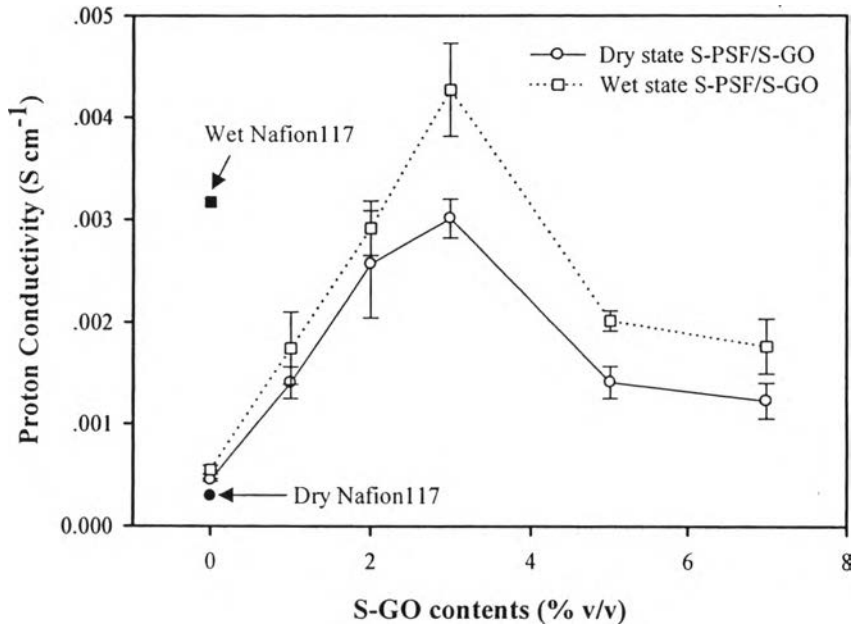

Figure 4.12 Proton conductivity of the S-PSF/S-GO composite membranes with a DS of 0.72 at 27 °C.

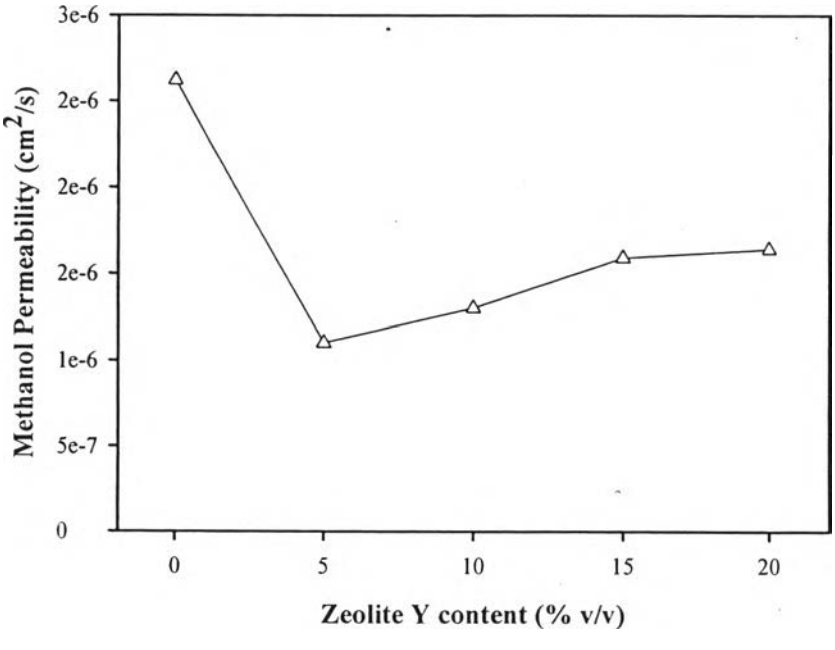

Figure 4.13 Methanol permeability at 70 °C of S-PSF and S-PSF/Zeolite Y composite membranes.

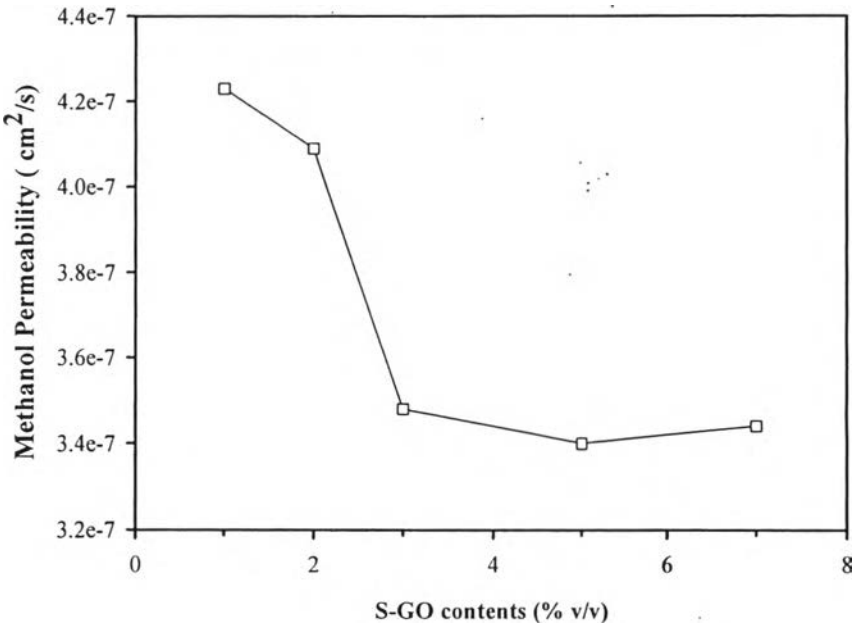

Figure 4.14 Methanol permeability at 70 °C of S-PSF and S-PSF/S-GO composite membranes.

Table 4.1 Proton conductivity and methanol permeability of S-PSF and composite membranes in the wet state at room temperature

PEM	Water Uptake (%)	d (cm)	R (Ω)	σ ($S.cm^{-1}$)	Methanol Permeability ($cm^2.s^{-1}$)	Membrane Selectivity ($s.S.cm^{-3}$)
Nafion 117	16.30	0.0178	0.18	3.17×10^{-3}	3.08×10^{-5}	1.03×10^{2}
S-PSF72	9.01	0.0202	3.28	5.46×10^{-4}	2.62×10^{-6}	2.08×10^{2}
S-PSF/5Y	15.02	0.0163	1.82	7.90×10^{-4}	1.10×10^{-6}	7.18×10^{2}
S-PSF/10Y	15.35	0.0168	0.85	1.74×10^{-3}	1.30×10^{-6}	1.34×10^{3}
S-PSF/15Y	20.88	0.0184	0.70	2.33×10^{-3}	1.59×10^{-6}	1.47×10^{3}
S-PSF/20Y	22.07	0.0186	1.11	1.52×10^{-3}	1.64×10^{-6}	9.27×10^{2}
S-PSF/1S-GO	10.80	0.0189	0.98	1.74×10^{-3}	4.23×10^{-7}	4.11×10^{3}
S-PSF/2S-GO	22.13	0.0192	0.59	2.92×10^{-3}	4.09×10^{-7}	7.14×10^{3}
S-PSF/3S-GO	22.33	0.0193	0.40	4.27×10^{-3}	3.48×10^{-7}	1.23×10^{4}
S-PSF/5S-GO	10.50	0.0190	0.83	2.02×10^{-3}	3.40×10^{-7}	5.94×10^{3}
S-PSF/7S-GO	3.86	0.0171	0.94	1.76×10^{-3}	3.44×10^{-7}	5.12×10^{3}
S-PSF/3S-GO /12Y	17.69	0.0182	0.41	4.01×10^{-3}	3.68×10^{-7}	1.09×10^{4}
S-PSF/3S-GO /15Y	15.20	0.0188	0.53	3.16×10^{-3}	3.33×10^{-7}	9.49×10^{3}

Note: S-PSF = Sulfonated polysulfone with the DS of 0.72 or pristine S-PSF
Y = Zeolite Y
S-GO = Sulfonated graphene oxide

For example:

S-PSF/5Y = S-PSF with 5 %v/v of zeolite Y content
S-PSF/5S-GO = S-PSF with 1 %v/v of sulfonated graphene oxide content
S-PSF/3S-GO/12Y = S-PSF with 3 %v/v of sulfonated graphene oxide and 12 %v/v of zeolite Y content

Table 4.2 Mechanical properties of S-PSF and composite membranes at 27 °C

Sample	Tensile Strength (MPa)	Yield Strain (%)	Young's Modulus (MPa)
Nafion 117	11.0 ± 0.4	24.1 ± 1.9	185 ± 10
PSF	39.9 ± 1.7	7.7 ± 0.9	921 ± 85
S-PSF72	28.4 ± 5.4	6.1 ± 0.6	844 ± 156
S-PSF/5Y	26.1 ± 5.4	4.3 ± 0.8	1011 ± 108
S-PSF/10Y	25.5 ± 2.1	4.5 ± 1.4	1212 ± 81
S-PSF/15Y	15.7 ± 1.3	3.4 ± 0.4	1208 ± 65
S-PSF/20Y	21.4 ± 4.5	2.7 ± 0.4	3205 ± 150
S-PSF/1S-GO	29.4 ± 2.8	5.4 ± 0.5	873 ± 77
S-PSF/2S-GO	36.5 ± 2.9	4.4 ± 0.6	907 ± 123
S-PSF/3S-GO	40.1 ± 1.9	3.4 ± 0.1	947 ± 67
S-PSF/5S-GO	44.0 ± 2.9	2.8 ± 0.3	1050 ± 78
S-PSF/7S-GO	48.9 ± 2.5	2.6 ± 0.12	1187 ± 66
S-PSF/3S-GO/12Y	14.9 ± 3.8	2.3 ± 0.8	1209 ± 102
S-PSF/3S-GO/15Y	13.5 ± 4.1	2.0 ± 0.9	1383 ± 96

Note: S-PSF = Sulfonated polysulfone with the DS of 0.72 or pristine S-PSF
Y = Zeolite Y
S-GO = Sulfonated graphene oxide